MOBILITY OF ROCK AVALANCHES TRIGGERED BY UNDERGROUND NUCLEAR EXPLOSIONS

V.V. ADUSHKIN[1]
Institute of Geospheres Dynamic, Russian Academy of Sciences
Moscow, Russia Leninskiy Avenue 38/6, Moscow 117334, Russia

Abstract

Several large rockslides and rock avalanches ranging in volume from 10^5 m^3 up to 10^8 m^3 were triggered by underground nuclear explosions at the Novaya Zemlia test site. Rapid filming of rock avalanche formation allowed direct measuring of the velocities of debris spreading. Dynamics of two case studies derived from the real time observations and from the analysis of debris morphology and grain size composition is discussed in details. Factors determining runout of artificial rock avalanches such as variability of debris grain size composition and topography of the transition and deposition zones are examined. Relationships of rock avalanche runout and their volume are determined and compared with those of the natural events of different origin. Critical conditions of slope failure occurrence depending on intensity of seismic effects of the explosions and slope angles are examined as well.

1. Introduction

Major rockslides, the volumes of which exceed few millions m^3 are characterised by flow-like debris motion when dry material moves as a liquid. Their runout can be much larger than fall height, sometimes exceeding ten kilometres, and deposits can cover tens and even hundreds square kilometres, and cause severe disasters in populated regions. The phenomenon is known as rock avalanche. Such catastrophic events occurred in the Alps [1, 12], Mackenzie Mountains [8], Tien Shan [11] and other mountain systems [7, 9, 11, 13, 23].

That is why study of rock avalanche phenomenon should be considered as an important and actual task of geomechanics and engineering geology. Numerous models have been proposed to explain mechanism of their extra-mobility. Some of these models explain reduction of apparent friction by influence of air [17], water [19], dust [14] and saturated soil [22]. Reliability of these models was examined, in particular, by Erismann [10] and Hungr [15]. Other models explain long runout of large dry rock avalanches, without any lubricants. Campbell [5] and Campbell et al. [6] proposed that low friction may be explained by granular mechanics. Melosh [20] developed theory of acoustic fluidisation that explain this phenomenon as the reduction of friction coefficient due to elastic acoustic vibrations in the rock avalanche body during its high-speed motion. In this model debris has a power-law shear-stress/strain-rate dependence similar to that of

[1] *E-mail:* dir@idg.chph.ras.ru

S.G. Evans et al. (eds.), Landslides from Massive Rock Slope Failure, 267–284.

a vibrating sand. A systematic, although limited, attempt to derive equivalent fluid parameters was made by Hungr and Evans [16]. Using a dynamic model, configured with Bingham friction and Voellmy rheologies, they obtain the best possible simulation of the deposits length as well as of their velocities and thickness.

Elaboration of the reliable mechanical models of rock avalanche formation and motion and their numerical simulation require objective input data. Such data can be obtained in the course of the detail field measurement of the deposits' geometrical parameters, study of the geological structure of the rock massifs and of the mineralogical and grain size composition of the debris. Very informative data can be obtained by the real time observations of the process, especially by filming of a rock avalanche during its motion. Systematic observations of rock slope failures and of the evolution of 'secondary' effects of underground nuclear explosions in rock massifs have been carried out at the Novaya Zemlya nuclear test site (Figure 1). As far as both time and place of rock slope failure were known in advance, it gave a chance to record whole process and to determine geometric parameters of the source zones and resultant deposits with high accuracy, rarely attainable in the study of the similar natural phenomena.

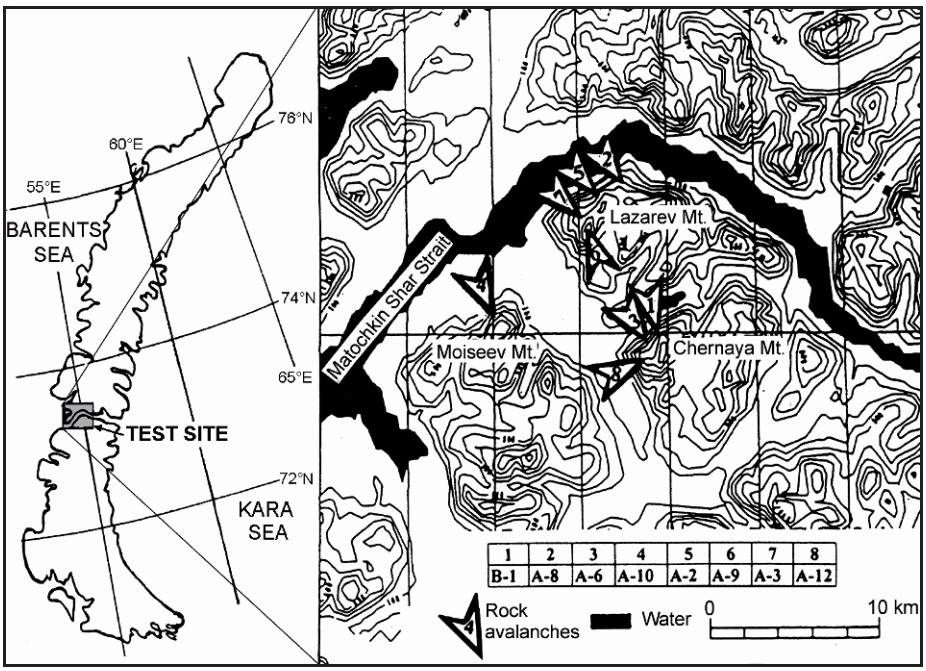

Figure 1. Schematic map of the Novaya Zemlia test site and location of rock avalanches triggered by underground nuclear explosions. Contour lines interval is 100 m.

2. Rock Avalanches Triggered by Underground Nuclear Explosions

In a number of cases underground nuclear explosions were accompanied by large-scale rockslides, some of which transformed into rock avalanches. It happened that such slope

failures caused significant material damage and destroyed registering equipment. To exclude rock avalanche formation in future testing, it had been necessary to determine the conditions under which rockslides occur and convert into rock avalanches and to predict their runout.

Processes of rock slope failure and avalanche motion were fixed by rapid filming from helicopters and ground observational points. Intensity of seismic shaking was measured by accelerometers and velocimeters. For better registration of surface motion after the camouflet explosions, special lights were burned at several points on the slope just before blasting and velocities of these lights' motion were measured. Volumes and areas of source zones and resultant deposits were calculated by surveying and aerial photography before and after the event with an accuracy of about 10-20%. Grain size composition of the resultant debris was studied by profile measuring of fragment dimensions on the surface of the rock avalanche deposits. Mineralogical composition of rocks was studied too. Rockslides ranging in volume from tens of thousands up to nearly one hundred million cubic meters [2] were recorded and studied. Parameters of largest events, which location is shown on Figure 1, are presented in Table 1.

Table 1. Dimensions of rock avalanches on the Novaya Zemlya test site.

Explosion	B-1	A-8	A-6	A-10	A-2	A-9	A-3	A-12
V (m^3)	$8{\cdot}10^7$	$2{\cdot}10^7$	$8{\cdot}10^6$	$5{\cdot}10^6$	$2{\cdot}10^6$	$5{\cdot}10^5$	10^5	$4{\cdot}10^4$
S (m^2)	$3.5{\cdot}10^6$	$7.5{\cdot}10^6$	$4{\cdot}10^5$	$2.6{\cdot}10^5$	$1.5{\cdot}10^5$	$6.5{\cdot}10^4$	$3{\cdot}10^4$	$2{\cdot}10^4$
h (m)	23	26.7	20	19.2	13.3	8	3.3	2
H* (m)	400	350	450	350	300	350	430	300
L* (m)	1900	900	1200	800-950	700	750	900	550
l (m)	1600	700	750	600	450	400	350	200
L*/H*	4.75	2.57	2.67	2.3-2.7	2.33	2.14	2.1	1.83

Here and below, 'V' and 'S' are the volume and the area of rock avalanche deposits, respectively; 'H*' is the height of the centre of gravity of the source zone; 'h' is the average thickness of the rock avalanche deposits; 'L*' is the maximum horizontal distance of the avalanche front from the centre of gravity of the source zone, and '*l*' is the length of rock avalanche deposits (Figure 2).

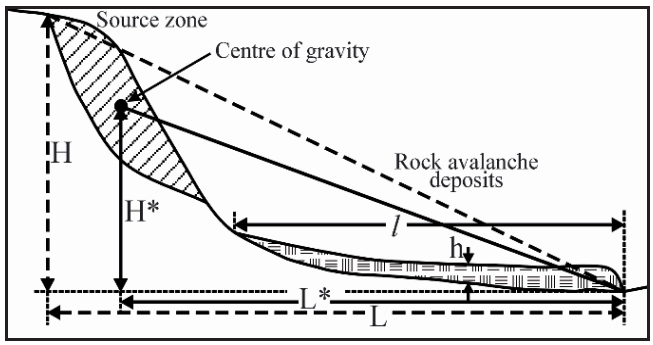

Figure 2. Relationships between parameters, traditionally used for rock avalanche description, and parameters, used in the present paper.

The site topography was similar for almost all explosions: the falling rock was able to move free down the slope and spread without significant confinements over the wide

valley bottoms, which are nearly horizontal or are inclined at an angle from 2º to 10º. It was found out that avalanche fronts moved much further than might be expected for a rockslide according to the law of dry friction. I must note that above definitions of 'H*' and 'L*' are traditionally used in our studies, though they differ from 'H' and 'L' parameters proposed by Heim [12] (see Figure 2). It should be taken into account in comparison of our data with estimates of rock avalanches' runout based on 'H' and 'L' values. However, our analysis show that in most of cases difference between H*/L* and H/L ratios does not exceed their scatters.

2.1. ROCK AVALANCHE TRIGGERED BY THE EXPLOSION B-1

The largest rock avalanche, $8 \cdot 10^7$ m^3 in volume (Figures 3-5), was created by the camouflet explosion in the tunnel B-1. The ridge at the test site was 850-900 m high and the crown of the scar rose up to 800 m. The steepest part of the slope, where its angle increased up to 40º-45º, was at the elevation from 300 to 500 m. Below it the slope angle gradually decreased to 5º-10º and to 2º-3º at the foot. The massif is composed of carbonaceous clayey shale with dolomite limestone interbeds, striking 110º-160º with dip angle 20º-30º. Rocks are intensively fractured: fractures' density varies from 5-10 to 30-50 per meter. Main fracture system coincides with bedding planes. Along the tunnel fault zones from 10-20 cm up to 1-2 m and, rarely 5-10 m thick were observed. The thickness of scree varies from 0.1-1 m on the slope to 5-6 m at its foot. Permafrost spreads inside the massive up to 500-600 m with constant temperature –4ºC. The subsurface zone 10-15 m thick is exposed to annual temperature fluctuation, decreasing inside the massif.

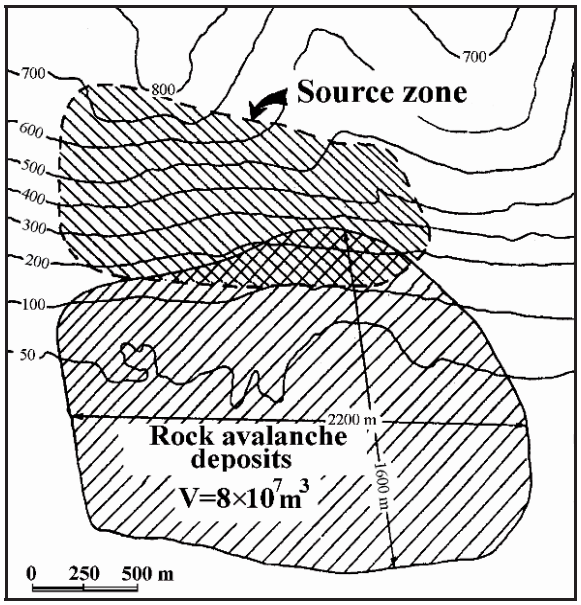

Figure 3. Schematic map of the source zone and of the deposition area of the B-1 rock avalanche. Contour lines correspond to the pre-failure relief.

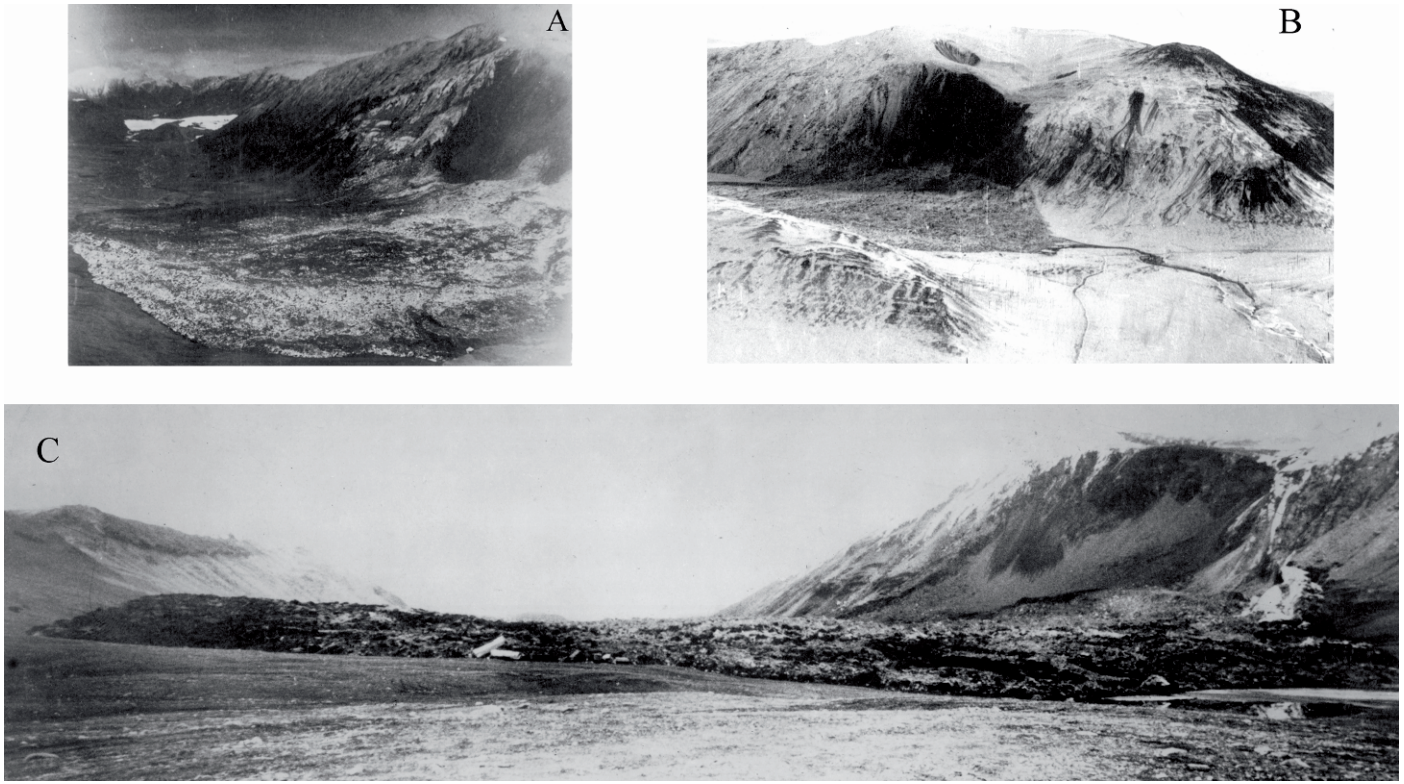

Figure 4. Photographs of the rock avalanche $8 \cdot 10^7$ m^3 in volume formed after the underground nuclear explosion in the tunnel B-1. A and B – views from helicopter; C – view from the downstream part of the Zhuravlevka River valley.

Figure 5. Aerial photo of the rock avalanche $8 \cdot 10^7$ m^3 in volume created by explosion in the tunnel B-1. White rectangle marks area shown on Figure 3; О$\sqcap$ -2,3,8 – control points used for survey.

Topographic sketch on Figure 3 shows the position of the source zone which occupied almost the whole mountainside and the final position of the rock avalanche deposits. Average depth of the scar that originated on the slope was about 80 m. Rock avalanche formed deposits up to 1.6 km long while L* was 1.9 km. Its width along the slope foot was 2.2 km, and thickness of the deposits varies from 10-20 m to 30-50 m. Rock avalanche covered $3.5 \cdot 10^6$ m^2, and its average thickness was calculated as 23 m.

This rock avalanche spread over the depositional area rather uniformly, so that the ratios of its area and width and those of source zone were 2.5 and 1.3 respectively. Rock avalanche debris blocked a rather wide valley of the Zhuravlevka River (the valley width at that place is 2 km approximately) and formed an artificial Nalivnoe (Im-

pounded) Lake, approximately 1×2 km in size, which still exists several tens of years after its formation. Filtration rate through the dam's body varies so that the spring flood does not overtop dams crest and, on the other hand, lake exists during low water period.

Main morphological features of the rock avalanche can be seen on Figure 5. Two morphological zones can be distinguished in the deposits. Larger frontal part of rock avalanche is characterised by radial alternating ridges and furrows. In contrast, its proximal part is formed by transverse ridges. At the lower part of the proximal zone there is a depression striking along the slope, that is marked by the deep bay of the Nalivnoe Lake. Basing on the above morphology, I assume that debris came to a halt first at its proximal part. Sequential stop of the tailing portions of debris, probably due to momentum transfer from them to distal portions of debris (similar to the mechanism proposed by Van Gassen and Cruden [25]) finally caused the stop of the entire mass of rock avalanche. Along the distal rim of rock avalanche debris, where it started to ascend the opposite slope, thickness of the deposits significantly increase. This frontal zone is characterised by more 'chaotic' micro-morphology. It can be also seen that rock avalanche expanded downstream the river valley more than upstream, and that the chaotic zone is much wider at the downstream limit of the rock avalanche (see Figure 5).

Since in the time of explosion was known with high accuracy, the whole process of slope failure and rock avalanche motion was filmed and motion parameters were derived. Figure 6 presents the graph of the velocity of the rock avalanche front motion measured from filming data.

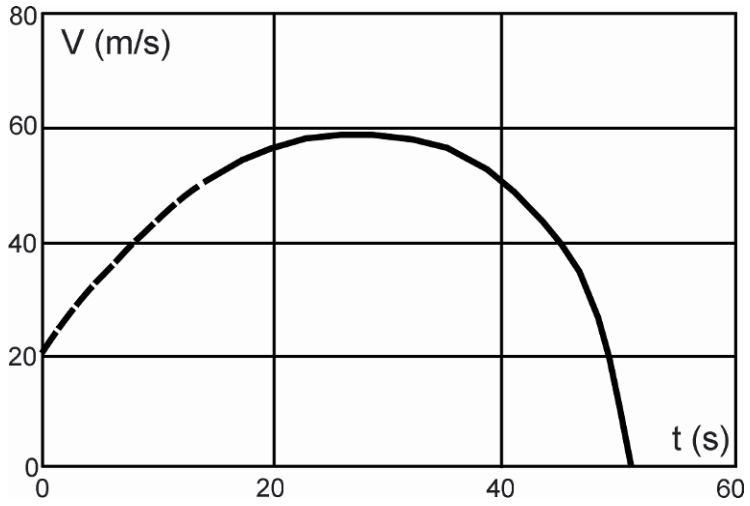

Figure 6. Front velocity of the B-1 rock avalanche as a function of time. Dashed line corresponds to that period of the rock avalanche motion when its front was masked by dust cloud.

Apparently, the debris velocity and, thus, its kinetic energy increased during first 15-20 seconds of motion when rock mass moved downslope. During this period it was seen that material that formed the slope surface settled down faster then deeper units. After 20-25 seconds, at a distance of about 1.0-km from the slope foot, the rock avalanche

front was formed, which velocity reached maximum value of 60 m/s (about 220 km/s). On the surface of the frontal part of moving rock avalanche we recognised debris that originated from rocks, which rested initially at the uppermost part of the slope. It was found out due to snow spots, because before the explosion snow covered only the very top of the mountain. High, almost maximal velocity of front motion remained for about 20 seconds. Assuming that the entire moving debris had the velocity close to the maximal, we found that kinetic energy of the avalanche (E_k) was about half of the potential energy of the rock mass involved in slope failure (E_p): $E_k \approx 0.5\ E_p$. It means that other half of potential energy was already spent on friction and rock destruction during rock avalanche motion. Avalanche stopped 50 seconds after the explosion. Therefore rock avalanche front came to a halt rather abruptly, approximately in 10 seconds (see Figure 6). Such abrupt decrease of the velocity and termination of motion should be considered as characteristic feature of rock avalanche motion.

2.2. ROCK AVALANCHE TRIGGERED BY THE EXPLOSION A-10

Rather unusual rock avalanche was triggered by seismic shaking after the powerful underground camouflet explosion in the tunnel A-10. Failure took place at the steepest part of the slope due to seismic effect of the explosion. Rock massif in the source zone is composed of terrigenous metasediments of the Silurian age, mainly mica schist, crystalline schist and mica-crystalline schist. Schistosity dips at an angle of 40º-60º in the same direction as the slopes' inclination. The total volume of the rock avalanche was about $5 \cdot 10^6$ m^3. The pre-failure site topography can be seen on Figure 7.

On the film that was made during the explosion and subsequent slope failure it was seen that in the beginning of motion the detached rock mass moved as a single unit and later subdivided into two parts with volumes ratio of approximately 1:4: Avalanche-1, 10^6 m^3 in volume, and Avalanche-2, $4 \cdot 10^6$ m^3 in volume (Figures 8 and 9). Their main geometrical characteristics are presented in Table 2.

Table 2. Geometrical parameters of the Avalanches 1 and 2 triggered by the A-10 explosion.

Parameters	V (m^3)	S (m^2)	h (m)	H* (m)	L* (m)	*l* (m)	L*/H*
Avalanche-1	10^6	$9.7 \cdot 10^4$	10	350	950	600	2.71
Avalanche-2	$4 \cdot 10^6$	$1.6 \cdot 10^5$	25	350	800	500	2.28

Gravity centres of both parts of rock avalanche were nearly at the same elevation of 350 m, though the crown of the scar above Avalanche-1 was 45-50 m higher. The average slope angle (30º-35º) and seismic intensity characterised by the maximum mass velocity (10-25 m/s), were generally the same for both avalanches. Both avalanches moved along unconfined surface and stopped on the valley bottom dipping 7º-9º.

The main difference between the two parts of this rock avalanche is their potential energy corresponding to the volume of each part. One could expect larger runout for Avalanche-2 due to its larger potential energy. But in the case we can see reverse situation: runout of Avalanche-1, with smaller volume, is approximately 1.2 times larger than the runout of Avalanche-2 that is 4 times larger in volume. Similarly, the L*/H* value for Avalanche-1 is bigger that that of Avalanche-2 also by a factor of 1.2.

Although the Avalanche-2 is 4 time bigger than the Avalanche-1, it covered the area only 1.6 times larger. It is caused by essentially smaller thickness of the Avalanche-1

deposits, which is 2.5 times less than that of the Avalanche-2 on an average. I should also note that thickness of the Avalanche-1 deposits is generally the same along its entire depositional area, while the Avalanche-2 is much thicker at its proximal part then at the distal one. Partially it can be explained by influence of relief: at the end of its path Avalanche-2 moved along small gully (see Figure 7). According to our experience channelling should lead to bigger runout of debris (the same was mentioned by Nicoletti and Sorriso-Valvo [21] for natural events). However, in our case situation is opposite, perhaps due to small extent of channelling at this site, as far as gullies' depth (10-15 m) was less than debris thickness and, thus, could not affect its motion significantly.

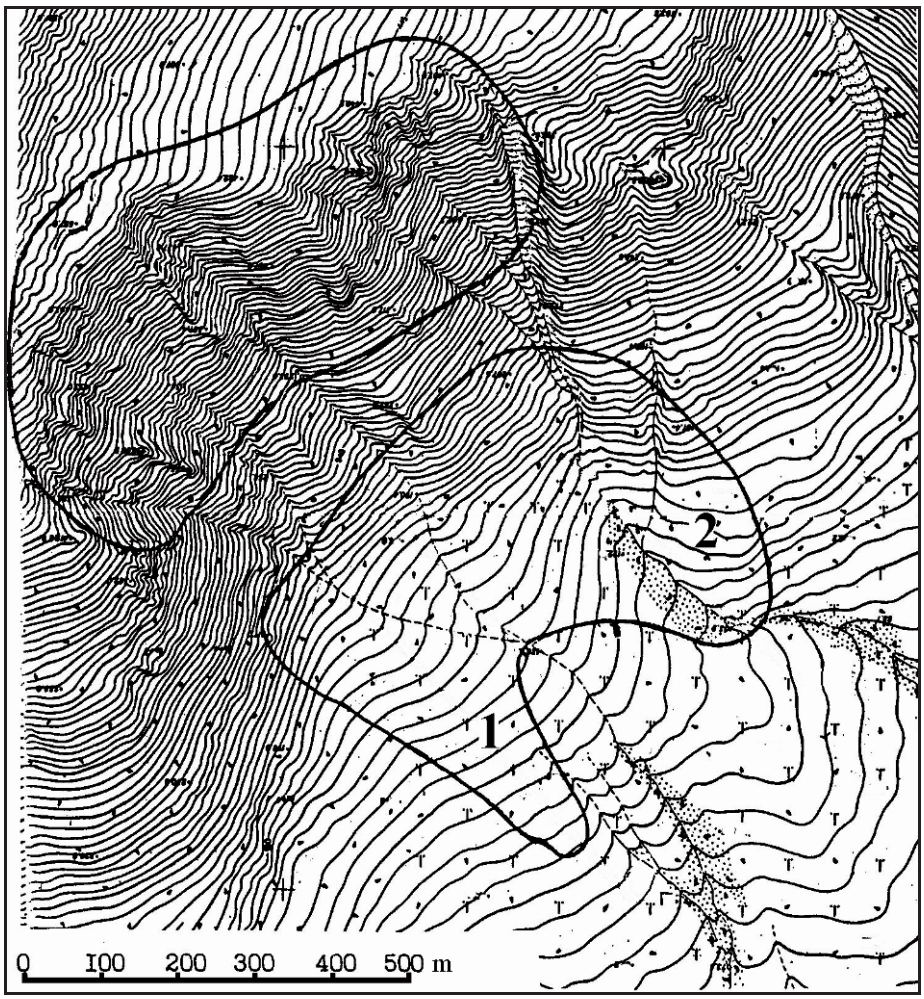

Figure 7. Topographic map showing pre-failure relief and configuration of the source zone and deposition area of the rock avalanche formed after the underground nuclear explosion in the tunnel A-10. Contour lines interval is 5 m. **1** and **2** – Avalanches-1 and 2, respectively.

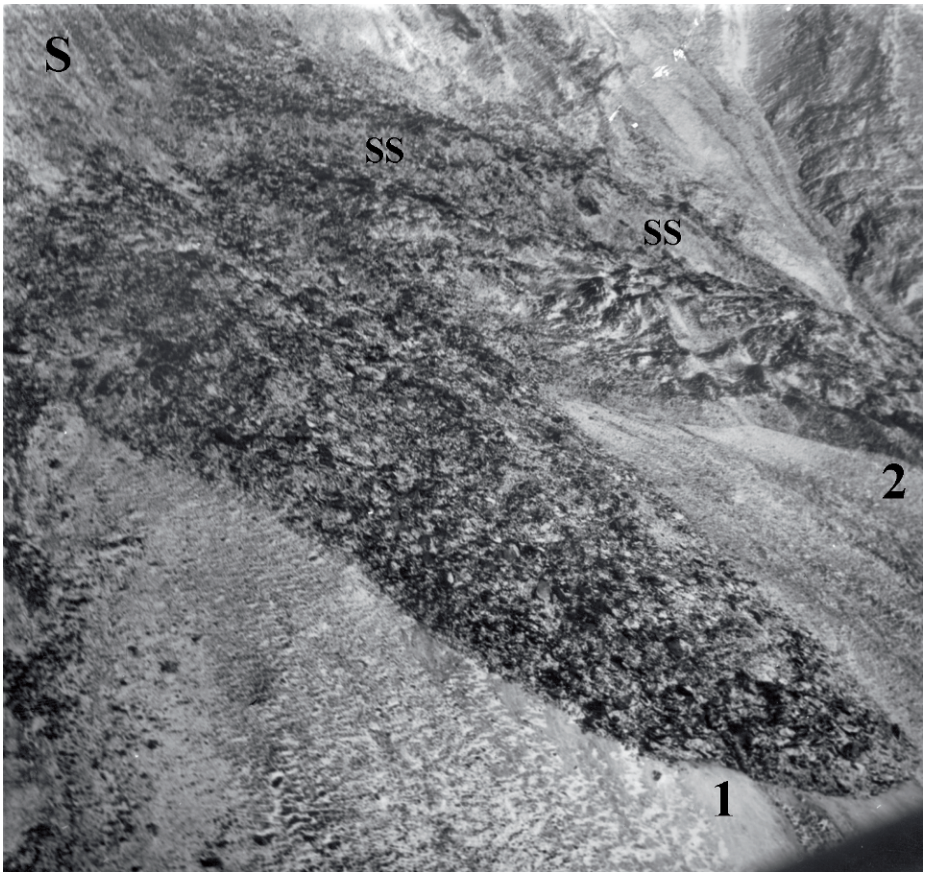

Figure 8. Oblique aerial view of the A-10 rock avalanche. The Avalanche-1 is at the foreground (**1**); part of the Avalanche-2 is at the background (**2**); the foot of the source zone on the upper left (**S**), and the secondary scar of the Avalanche-2 is marked by (**SS**).

It was assumed that difference in runout might depend on the grain size distribution in the rock avalanche deposits, which is significantly different for these two parts of rock avalanche [3]. Rock fragments on the surface of the Avalanche-2 body are less than 1 m in size, and grain size distribution is characterised by rather small scatter with most abundant fraction of about 15-30 cm. On the other hand, deposits of Avalanche-1 consist of debris with more variable grain size, varying from a few centimetres to 5-10 metres (Figure 10). Difference between debris composition of Avalanches-1 and 2 can be attributed to the difference in the mineral compositions and rock structure due to local peculiarities of metamorphism.

However, other explanation of smaller runout of Avalanche-2 in comparison with Avalanche-1 can be proposed (A.L. Strom, Personal Communication, 2002). As could be seen on Figure 7, transition from the slope at the foot of source zone to the deposition area is more smoothed above the Avalanche-1, where it coincide with a small gully, rather then above the Avalanche-2, with prominent steep massif between two gullies.

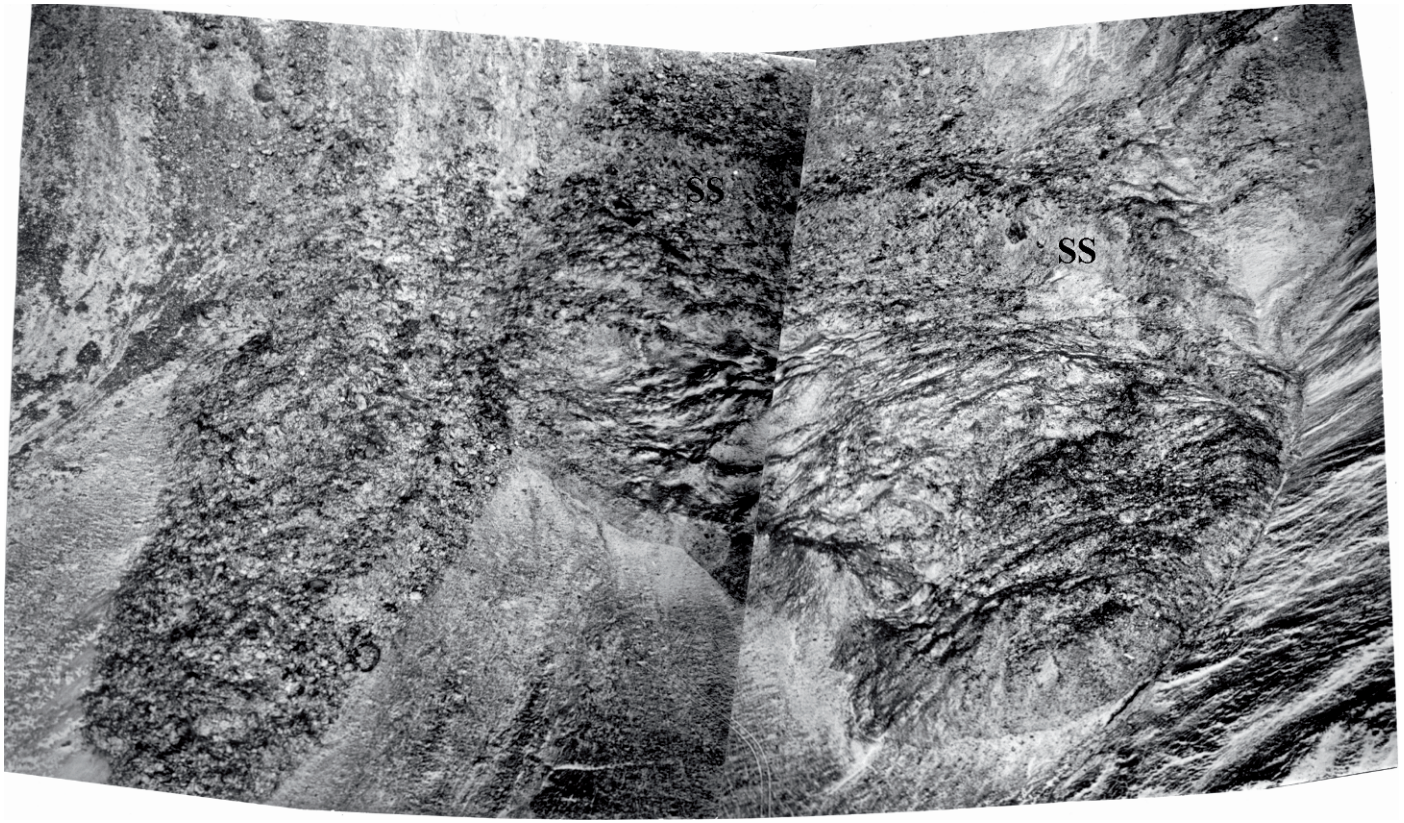

Figure 9. Combination of vertical aerial photographs of the rock avalanche formed after explosion A-10. The Avalanche-1 is on the left, the Avalanche-2 - on the right. Secondary scar above the tongue of the Avalanche-2 is marked by (**SS**).

It caused different stile of motion of corresponding parts of the rock avalanche. The Avalanche-1 was completely involved in the flow-like motion while the Avalanche-2 can be divided by secondary scar (marked by 'SS' on Figures 9 and 10) into proximal unit that accumulated at the slope's foot and avalanche unit. Similar debris distribution is typical of numerous natural events [24]. Thus, partial involvement of the Avalanche-2 debris in the flow-like motion could lead to its smaller runout.

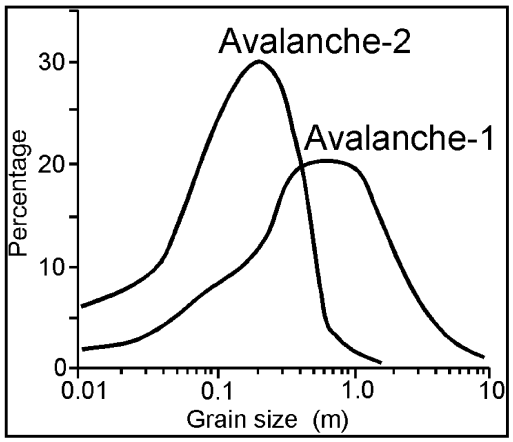

Figure 10. Grain-size distribution of debris on the surface of the Avalanches-1and 2 of the A-10 event.

Processes of slope failure and avalanche motion at the A-10 test site were fixed by rapid filming. Figure 11 shows successive profiles of the Avalanche-1, as it moved downslope, derived from the film. In the beginning, rock avalanche was obscured by a cloud of dust, which followed the slide. Contour labelled (1) on Figure 11 is the first one when rock avalanche front became visible as it passed through the front of the dust cloud, and successively numbered contours represent later stages in rock avalanche evolution. Based on these data the velocity of the avalanche front was determined.

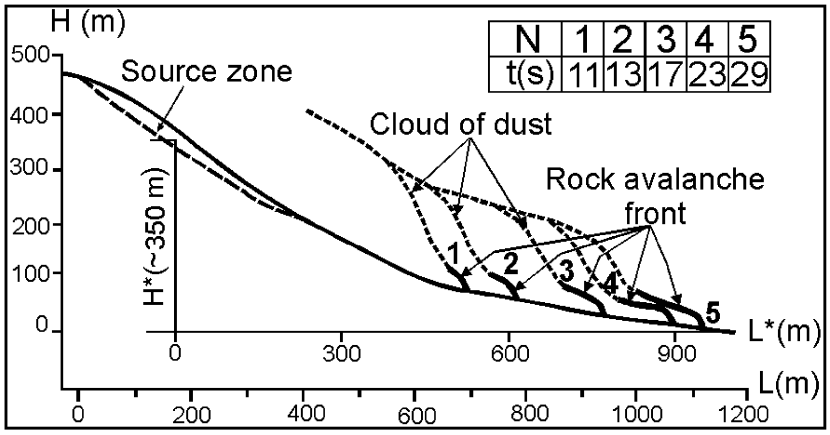

Figure 11. Dynamics of the Avalanche-1 derived from the rapid film. Numbers correspond to the position of rock avalanche front at the specified time points (in seconds) after the explosion.

This part of sliding mass accelerated during its motion along the first 500 m of the runout that started on the slope of 35º and continued until the slope angle decreased up to 15º. Then rock avalanche decelerated. Final stage of motion occurred on the slope, which angle varies from 7º to 10º. The maximum velocity of the Avalanche-1 front reached nearly 40 m/s and lasted for about 10-15 seconds (Figure 12). Assuming, that the whole mass of debris had maximum velocity at this period, its kinetic energy (E_k) could be estimated as about 0.4 of the potential energy of the descended rock massif (E_P). Thus, at this stage of rock avalanche motion more then half of the entire energy dissipated due to friction and rock destruction. Total duration of slope failure and rock avalanche motion was ~30 seconds.

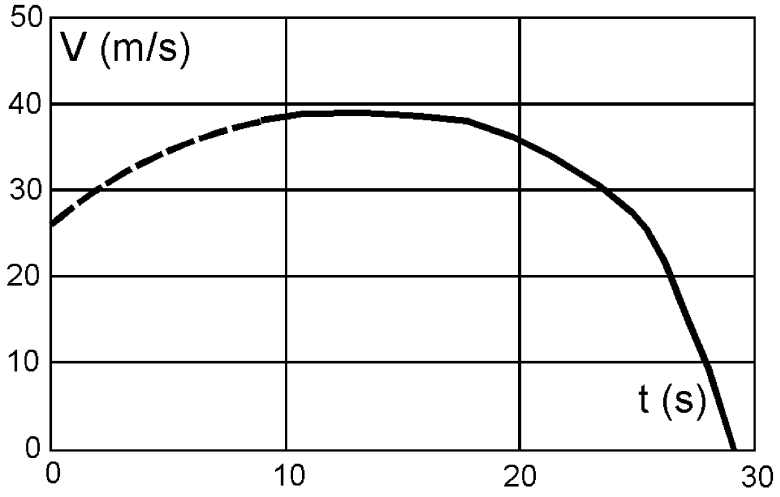

Figure 12. Front velocity of the Avalanche-1 as function of time. Dashed line corresponds to that part of the avalanche motion when its front was masked by dust cloud.

2.3. CRITICAL CONDITIONS OF LARGE-SCALE ROCK SLOPE FAILURE

Parameters of seismic motion on the slopes caused by powerful underground explosions. were registered by accelerometers and velocimeters. Maximum particle (mass) velocity on the slopes dipping 30º-50º, where large-scale failures occurred, ranged from 8 m/s up to 25 m/s and average acceleration value, measured during such explosions as A-10 or B-1, varied from 10 to 30 g. On the basis of these data critical conditions of large-scale rock slope failure, depending on the intensity of seismic effects and on the slope angle, were determined (Figure 13). Three dashed curves on Figure 13 reflect data obtained in the course of field measurements at the test sites with different slope steepness, geological structure and rock strength and firm line corresponds to the empirical relation of the threshold combination of mass velocity and slope angel described by equation 1.

$$U_{cr} = \frac{5.2}{tg(\alpha - 25^{\circ})} \text{ (m/s); } \alpha > 25^{\circ} \qquad (1)$$

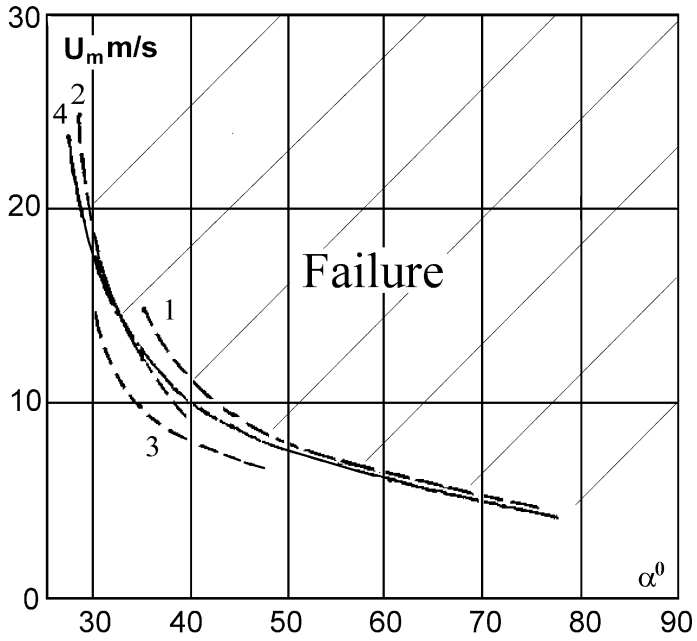

Figure 13. Critical conditions of the large-scale rock slope failure. 1-3 – empirical data on mass velocity of seismic waves measured on the slopes of different steepness at the test sites: 1 – Lazarev Mountain, 2 – Moiseev Mountain, 3 – Chrnay Mountain. 4 – graph of equation (1); hatched zone corresponds to failure conditions.

Function (1) can be applied for large-scale events only, when linear dimensions of the area on the slope affected by seismic wave with mass velocity U_{cr} and higher, is not less than 10^2-10^3 m.

2.4. RELATIONSHIPS OF ARTIFICIAL ROCK AVALANCHES PARAMETERS

Data obtained by rapid filming of rock avalanches, triggered by the B-1 and the A-10 explosions show that their fronts moved with velocities up to 40-60 m/s. Under the same conditions, the larger is the rock avalanche mass, the higher is its front velocity.

Distance of rock avalanche front motion is considered as the main characteristic of this phenomenon. It is determined by the kinetic energy value, which rock mass gains while it descend moving downslope under the influence of gravity force. It is evident that L*/H* ratio of rock avalanches, triggered by seismic effect of underground explosions, that have roughly similar H* values (300-450 m), distinctly increase with increase of avalanche volume. Rock avalanches with volumes of 10^4-10^5 m^3 have the L*/H* ratio about 2. Rock avalanches, which volume is of the order of 10^8 m^3 have the L*/H* ratio up to 5 (Figure 14-A). It implies that with increase of slope failure volume, style of debris motion changes and becomes similar to the motion of the viscous fluid.

Fluid-like motion of artificial rock avalanches that spread over unconfined surface becomes apparent from the analysis of the relationship between average thickness of the deposits and their volume (Figure 14-B). While volume grows from 10^4 up to 10^6 m^3,

the average thickness of rock avalanche deposits gradually increase. For volumes exceeding 5×10^6 m^3, average thickness of the deposits reach 20-25 m and further increase of rock avalanche volume is not accompanied by proportional thickening of deposits. It means, that in the case of large rockslide, debris maintain avalanche-like motion until its thickness decrease up to some critical value. After that, resistance to motion increases abruptly being governed by dry friction, and rock avalanche stops.

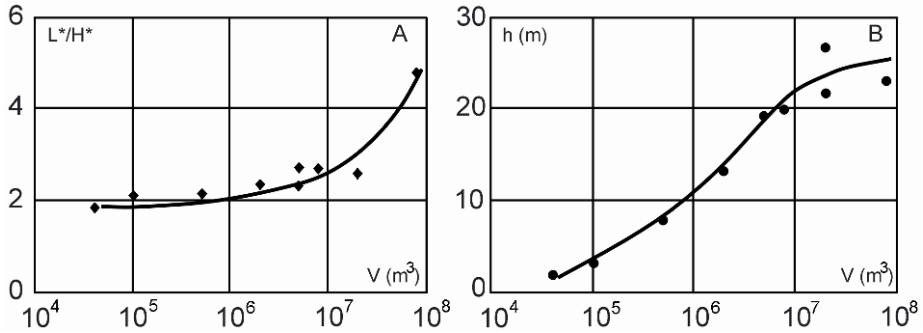

Figure 14. Length of rock avalanche fronts runout (A) and average thickness of deposit (B) as function of their volume.

3. Comparison With Natural Events

To analyse motion of rock avalanches of larger volumes we used data on several well-known natural events, which volumes range from 10^7 up to $n\times10^{10}$ m^3 [23, 26]. Some of them are comparable in size with the largest artificial avalanches at the Novaya Zemlya test site and have L/H ratio of the same order ranging from 3 to 5 [23]. As noted above, for general qualitative comparison it is acceptable to use both L and H, and L* and H* values (see Figure 2) and corresponding ratios. Length of runout of larger natural rock avalanches involving cubic kilometres of debris, is much bigger – up to 13-16 km [23] and corresponding L/H values exceed 10. Several rock avalanches associated with volcanic eruptions, such as the Shiveluch, Bezymyannyi and Kamen in Kamchatca and the St. Helens event in the U.S.A., were analysed too.

One more group of slope failures, resulting in the avalanche-like motion, which was utilised for the comparison of the artificial and natural rock avalanches, is failure of the rock waste dumps of the Central mine in the Khibini Mountains [18]. Dumps are stacked on the steep slopes of the Rosvumchorr Plateau at elevation of 900-1000 m a.s.l. Slope angles of the plateau reach 30-50°. As the waste accumulates sudden collapses of debris mixed with ice and snow occur, creating rock-ice avalanches. Parameters of the largest rock-ice avalanches are presented in Table 3. It should be noted that rock-ice avalanches are extremely mobile comparatively to their volumes and, thus, pose a significant threat.

Correlation of L/H as well as L*/H* and *l*/H* ratios of artificial and natural rock avalanches of different origin versus their volumes are shown on Figure 15. It represents general relationships of these parameters that fit to the same equation both for natural and artificial events.

Table 3. Parameters of the rock-ice avalanches.

V (m^3)	$2{\cdot}10^6$	$7{\cdot}10^5$	$1.5{\cdot}10^6$	$1.3{\cdot}10^6$	$2.4{\cdot}10^6$	$2.6{\cdot}10^6$	$6{\cdot}10^6$	$3{\cdot}10^5$	$4{\cdot}10^6$
L* (m)	1100	400	1000	500	1100	900	3000	240	1600
H* (m)	400	250	400	250	400	370	650	170	500
L*/H*	2.7	1.6	2.5	2.0	2.7	2.4	4.6	1.4	3.2

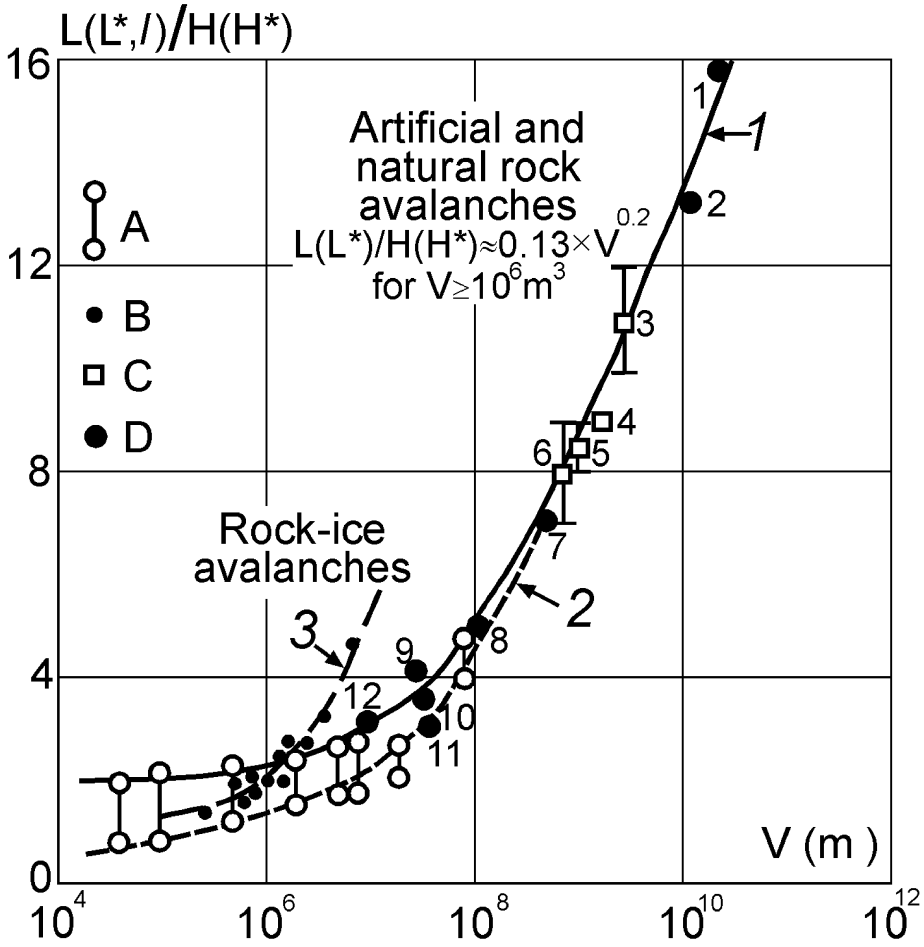

Figure 15. Dependence of the rock avalanche length to fall height ratio, versus their volume (after [2], modified). Key to legend: A – rock avalanches triggered by underground nuclear explosions (see table 1). Upper circle – L*/H* value, lower circle – *l*/H* value. B – rock-ice avalanches at the Khibini Mountains (L*/H* values). C – volcanic rock avalanches (L/H values with their scatter). D – natural non-volcanic rock avalanches (L*/H* values). The following natural events are enumerated: 1- Saidmarreh, 2 – Flims, 3 – St. Helens volcano, 4 – Shiveluch volcano , 5 – Kamen volcano, 6 – Bezymyannyi volcano, 7 – Khait, 8 – Aini, 9 – Goldau, 10 – Frank, 11 – Madison, 12 – Elm. Curves 1-3 are explained in the text.

Curve 1 on Figure 15 is drawn through a set of points that represent rock avalanches at the Novaya Zemlya test site and natural rock avalanches that moved in the unconfined environment. For rather small volumes (10^4-10^6 m^3), the L*/H* ratio is practically

constant and equal to ≈2. In the range of volumes $V=10^7–10^8$ m^3, there is a good agreement between data on rock avalanches of explosive and natural origins. For bigger volumes, curve 1 also fits well with data on both volcanic and non-volcanic events. For $V\geq10^6$ m^3 this curve can be described by the empirical function:

$$L(L^*)/H(H^*) = 0{,}13V^{0,2} \quad (2)$$

Curve 2 on Figure 15 reflects growth of *l*/H* ratio versus rock avalanche volume for the artificial events. For volumes more than 10^8, when length of unconfined debris apron significantly exceeds dimensions of the source zones, it becomes very close to the curve 1. Shape of these curves show that massive rock slope failures in which more than one million of cubic meters of rocks are involved, are accompanied by a peculiar scale effect that leads to anomalous mobility of debris and a to corresponding increase of rock avalanche runout.

Lastly, the rock-ice avalanches formed on waste dumps in the Khibini Mountains have much higher mobility, demonstrated by curve 3 on Figure 15. It can be assumed that presence of the ice and snow reduces the resistance force of such avalanches and their mobility starts growing at lower volumes.

4. Conclusions

Real-time observations of the processes of massive rock slopes failure and rock avalanches formation at the Novaya Zemlia nuclear test site provided data for better understanding of this hazardous phenomena. Numerous artificial rock avalanches ranging in volume from 10^5 m^3 up to 10^8 m^3 have been studied in details.

Critical conditions at which rock slopes' failure occur, depending on mass velocity caused by seismic waves and on slope angle, have been established for seismic effects of underground nuclear explosions. They can be applied for natural conditions too, especially in the areas, where strong motions, corresponding to 9 or more points of the MM or MSK scales are expected.

Direct measurement of rock avalanches front velocities show that they reach 40-60 m/s and that rapidly moving debris came to a halt in few seconds when its velocity decreases from more than 90 km/h up to zero. It proves the indirect observations, indicating the abrupt stop of natural rock avalanches. It was also found out that when rock avalanche front velocities were maximal, more then half of the initial energy of descending rock mass already dissipated due to friction and debris fragmentation.

Differences in geometrical parameters of two parts of rock avalanche triggered by A-10 explosion allow proposing that grain size distribution of rock avalanche debris can affect their mobility. I hypothesise that rock avalanches composed of uniform material are less mobile than those composed of fragments more variable in size. However, it can not be excluded that the observed differences were due to peculiarities of the site topography, which caused different mass distribution in both parts of this rock avalanche.

Comparison of rock avalanches triggered by powerful underground explosions and both volcanic and non-volcanic large-scale natural events demonstrates that their high mobility obeys the same relationships and, thus, should be governed by the same me-

chanical processes. The empirical formula (2) and curves 1-3 on Figure 15 allow predicting roughly geometrical parameters of unconfined rock avalanches for the given volume and the height of collapse.

References

1. Abele, G. (1974) *Bergsturze in den Alpen*, Wissensch, Alpenvereinshefte, Munchen H. 25.
2. Adushkin, V.V. (2000) Explosive initiation of creative processes in nature. *Combustion, Explosion, and Shock Waves* **36**, No 6, 21-30.
3. Adushkin, V.V., and Spungin, V.G. (1998) The influence of granular structure of rockfalls on their speading along mountain slopes. In: *Proceedings of the third international Conference on Mechanics of Jointed and Faulted Rock. Vienna, Austria, 6-9 April 1998*, 541-546.
4. Adushkin, V.V., Rodionov, V.N., and Shcherbakov, S.G. (2000) Mechanism of the spontaneous generation of rock avalanches on mountain slopes. *Doklady Earth Sciences*, **373 A**, 958-959.
5. Campbell, C.S. (1989) Self-lubrication for long runout landslides, *J. Geology* **97**, 653-665.
6. Campbell, C.S., Cleary, P.W., and Hopkins, M. (1995) Large-scale landslide simulations: Global deformation, velocities and basal friction, *J. Geophys. Res.* **B100**, 8267-8283.
7. Costa, J.E., and Schuster, R.L. (1988) The formation and failure of natural dams, *Geol. Soc. Am. Bull*. **100**, 1054-1068.
8. Eisbacher, G.H. (1979) Cliff collapse and rock avalanches (sturzstroms) in the Mackenzie Mountains, northwestern Canada, *Can. Geotechnical J*. **16**, 309–334.
9. Eisbacher G.H., Clague J.J. (1984) *Destructive mass movements in high mountains: hazard and management. Ottawa*, Geological Survey of Canada Paper 84-16.
10. Erismann, T.H. (1986) Flowing, rolling, bouncing, sliding: synopsis of basic mechanisms, *Acta Mechanica* **64**, 101-110.
11. Fedorenko, V.S. (1988) *Mauntainous Rockslides and Rock Falls, their Prediction*, Moscow State University (in Russian).
12. Heim, A. (1932) *Der Bergsturz und Menschenleben*, Fretz und Wasmuth, Zurich.
13. Hewitt, K. (2001) Catastrophic rockslides and the geomorphology of the Hunza and Gilgit river valleys, Karakoram Himalaya, *Erdkunde* **55**, 72-93.
14. Hsu, K.J. (1975) Catastrophic debris streams generated by rockfalls, *Geol. Soc. Am. Bull*. **86**,129-140.
15. Hungr, O. (1990) *Mobility of rock avalanches*. Reports of the National Research Institute for Earth Science and Disaster Prevention, Tsukuba, Japan, **46**, 11-20.
16. Hungr, O., and Evans, S.G. (1996) Rock avalanche runout prediction using a dynamic model, in: *Proceeding 7 th International Symposium on Landslides*, Trondheim, Norway, 1996, Balkema, 233-238.
17. Kent, P.E. (1966) The transport mechanism in catastrophic rockfalls, *J. Geology* **74**, 79-83.
18. Krasnoselsky, E.V., and Kalabin, G.V. (1975) *Rock dumps on mountain slopes*, Nauka, Leningrad, (in Russian).
19. Legros, F. (2002) The mobility of long-runout landslides, *Engineering Geology* **63**, 301-331.
20. Melosh, H.J. (1979) Acoustic fluidization: a new geological process?, *J. Geophys. Res*., **84**, 7513-20.
21. Nicoletti, P.G. and Sorriso-Valvo M. (1991) Geomorphic controls of the shape and mobility of rock avalanches, *Geol. Soc. Am. Bull.* **103**, 1365-1373.
22. Sassa, K., Fukuoka H., Lee, J-H., Shoaei Z., Zhang, D., Xie, Z., Zeng, S, Cao, B. (1994) Prediction of landslide motion based on the measurement of geotechnical parameters, in: *Developement of a new Cyclic Loading Ring Shear Apparatus to study earthquake-induced-landslides. Report for Grant-in-Aid for Developmental Scientific Research by the Ministry of Education, Science and Culture, Japan (Project No 03556021)*, DPRI, Kyoto, 72-106.
23. Shaller, P.J. (1991) *Analysis and implications of large Martian and Terrestrial landslides*, Ph.D. Thesis, California Institute of Technology.
24. Strom, A.L. (2003) Morphology and internal structure of rockslides and rock avalanches; grounds and constraints for their modelling. This volume.
25. Van Gassen, W., and Cruden, D.M. (1989) Momentum transfer and friction in the debris of rock avalanches, *Can. Geotechnical J.* **26**, 623 - 628.
26. Voight, B., Landa, R.G., Glicken H., Douglass, P.M. (1983) Nature and mechanics of the Mount St.Helens rockslide-avalanche of the 18 May 1980. *Geotechnique* **33**, 243-273.